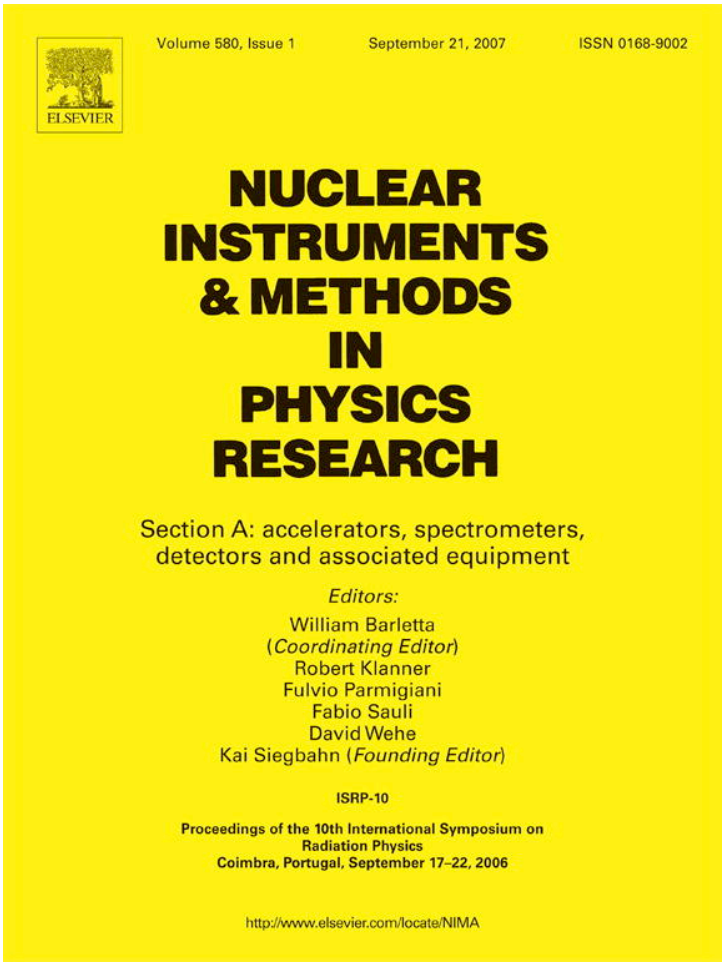

Available online at www.sciencedirect.com
ScienceDirect
ELSEVIER
Nuclear Instruments and Methods in Physics Research A 580 (2007) 33–36
NUCLEAR INSTRUMENTS & METHODS IN PHYSICS RESEARCH Section A
www.elsevier.com/locate/nima

Detection of faint X-ray spectral features using wavelength, energy, and spatial discrimination techniques

L.T. Hudson[a,*], J.D. Gillaspy[a], J.M. Pomeroy[a], C.I. Szabo[a], J.N. Tan[a], B. Radics[b], E. Takacs[b], C.T. Chantler[c], J.A. Kimpton[c], M.N. Kinnane[c], L.F. Smale[c]

[a]*National Institute of Standards and Technology, 100 Bureau Drive, Gaithersburg, MD 20899, USA*
[b]*University of Debrecen, Debrecen, Bem ter 18/a, H 4026, Hungary*
[c]*School of Physics, University of Melbourne, Vic. 3010, Australia*

Available online 22 May 2007

Abstract

We report here our methods and results of measurements of very low-signal X-ray spectra produced by highly charged ions in an electron beam ion trap (EBIT). A megapixel Si charge-coupled device (CCD) camera was used in a direct-detection, single-photon-counting mode to image spectra with a cylindrically bent Ge(2 2 0) crystal spectrometer. The resulting wavelength-dispersed spectra were then processed using several intrinsic features of CCD images and image-analysis techniques. We demonstrate the ability to clearly detect very faint spectral features that are on the order of the noise due to cosmic-ray background signatures in our images. These techniques remove extraneous signal due to muon tracks and other sources, and are coupled with the spectrometer wavelength dispersion and atomic-structure calculations of hydrogen-like Ti to identify the energy of a faint line that was not in evidence before applying the methods outlined here.

PACS: 32.30.Rj; 39.30.+w; 07.05.Kf; 07.85.−m

Keywords: X-ray spectroscopy; Highly charged ions; CCD imaging; Crystal spectroscopy; Cosmic ray removal

1. Introduction

Studies with highly charged ions are motivated by the growing interest in the fundamental mechanisms of radiation interactions with extreme states of matter and their wide array of potential applications. In the course of a program of precision X-ray metrology at the NIST Electron Beam Ion Trap, a wide variety of atomic systems have been studied that exhibit X-ray signal strengths spanning several orders of magnitude. In recent experiments we have used wavelength-dispersive and energy-dispersive X-ray spectroscopy to observe well-resolved intense resonance transitions as well as less-intense features while acquiring the spectra of hydrogen-like and helium-like medium-Z atomic systems.

In this report, we focus on the methods and instruments we have employed for obtaining good signal-to-noise (S/N) X-ray spectra in situations of very low signal strength. This has required the additional step of spatial discrimination by event size, measured in detector pixels of an area detector. As an example, these techniques are then applied to the observation of a faint X-ray line whose energy is obtained by reference to intense, nearby resonance lines of hydrogen-like Ti. More generally, these strategies can find use in other imaging and spectroscopic applications where features of interest are modest compared to the noise level.

2. Experimental method

In the present work, high resolution and favorable S/N are obtained in X-ray spectra by applying a combination of discrimination techniques. In the course of studying hydrogen- and helium-like Ti spectra, titanium is loaded into the NIST EBIT using a newly designed metal vapor

*Corresponding author. Tel.: +1 301 975 2537; fax: +1 301 975 3038.
E-mail address: larry.hudson@nist.gov (L.T. Hudson).

0168-9002/$ - see front matter © 2007 Elsevier B.V. All rights reserved.
doi:10.1016/j.nima.2007.05.034

vacuum arc [1] where it is trapped, highly ionized, and excited by an axially centered electron beam (25.7 kV, 150 mA). X-rays satisfying the diffraction condition of a Ge(2 2 0) cylindrically bent [2] crystal spectrometer [3] are dispersed and registered by a 1152 pixel × 1242 pixel CCD area detector used in direct detection mode. Individual images were integrated for 90 s. This insured the validity of single-photon counting per pixel while keeping the integrated thermal background of the chilled CCD (−40 °C) well below registered X-ray signals. Before and after a series of 80 images, a background image was acquired with the EBIT source high-voltage turned off.

A recorded image can be represented by a matrix of numbers wherein each element represents the charge accumulated in a particular pixel during the acquisition, digitized to 16 bits. The pixel intensities have contributions from many sources, many of which are relatively large but unrelated to the physical processes under study. Included in our raw CCD images are contributions due to: (1) X-rays from the EBIT that are diffracted by the crystal spectrometer and registered directly; in general, this could include higher-order diffraction contributions; (2) thermally integrated charge, superimposed with intrinsic fixed-pattern noise as well as patterns due to previous radiation history (damage) of each pixel; (3) electronic readout noise; (4) charge collected in CCD pixels due to energy losses by in-transit cosmic rays; and (5) a smooth, frame-to-frame level drift due to long-term temperature changes of laboratory acquisition electronics.

The following image manipulation and processing techniques can filter out sources (2)–(5) as well as 2nd-order diffracted X-rays, permitting the observation of even very faint, low-count-rate signals of the order of a mHz. A histogram of the pixel values of raw images is dominated by source (2) noise, and is largely removed by subtraction of a "source-off" image matrix from each of a series of images taken while the EBIT was "on" and producing the X-rays of interest. Any global level drift that may have occurred during a long measurement interval is then removed by an offset that aligns the histograms of pixel values of each frame. These histograms of background-subtracted images are dominated by a large number of pixel values that statistically fluctuate around zero, with a small number of pixels with higher values that are due to the X-rays of interest from the source under study as well as unwanted tracks due to energy losses from secondary cosmic rays (penetrating muons [4]). As usual in single-photon detection studies, the condition to achieve high S/N is that the real X-ray photons produce a signature that can be easily separated from the low-level noise. The energy resolution of our CCD is relatively coarse; for example, it is measured to be about 230 eV at Fe Kα (6.4 keV). Using the energy-dispersive content of the difference image, a prediscrimination is performed by replacing all pixel values that are well below the signal levels of interest with zero. This leaves mostly zero pixel values in each frame, permitting easy identification and discrimination of "clusters." A cluster is an event defined as essentially an island of one or more non-zero contiguous pixels surrounded by pixels of zero intensity.

Since the incident signal rate of interest is quite low in the present study, the cosmic-ray background signal is comparable to that from faint lines in the spectra. This background cannot be entirely removed by single-pixel energy-dispersive analysis in those cases where the energy deposited per pixel by the cosmic particle in transit is digitized with values similar to those falling in the energy window of the crystal spectrometer. Hence, we have imported a technique to identify and discriminate against multi-pixel events that we previously developed to analyze X-ray pin-hole image data from an electron cyclotron resonance ion source [5]. The algorithm finds clusters by recursively checking the vertical and horizontal nearest-neighbor pixels and tagging them if there is non-zero signal present. The number of pixels per cluster, and summed values of each pixel of the cluster, are tabulated for possible discrimination against cluster size or total energy. In the image matrix, the summed intensity is placed in the intensity-weighted center of the pixel coordinates, and the remaining pixel values within that cluster are replaced with zero. By additionally applying this spatial-discrimination technique, most tracks due to muons are eliminated while real X-ray events occupying more than one pixel (a few percent of the total) are added to the accounting that would have been excluded in single-pixel discrimination.

After applying these energy- and topological-discrimination techniques for enhancing S/N, the wavelength–dispersed spectrum is analyzed. In general, energy scales are established with calibrated angle-encoding schemes, X-rays of known or calculated wavelengths, modeling of crystal dispersion and source-detector geometry, relative X-ray or angle standards, or some combinations of the above. In the present work, the crystal dispersion and spectrometer geometry are used to identify two bright resonance lines of hydrogen-like Ti. The local energy scale thus established is then used to estimate the energy of a faint (mHz count rate) line that was not evident before applying energy and cluster discrimination.

3. Experimental results

X-ray emissions from highly ionized titanium were studied using a tunable X-ray spectrometer. Coarse tuning is provided by encoding the central screw of the spectrometer sine drive. For the present measurement, the encoder was set to correspond to a nominal X-ray energy of 6.5 keV, motivated in part by observation of unresolved structure in this region using a high-purity Ge detector.

Under the EBIT conditions described in Section 2, a series of 90 s images was acquired, usually in groups of 80, for a total integration time of about 64 h. Difference images were created, any drift reset, and prediscrimination performed by setting to zero all pixels with digitized values <40 (relative units). From an energy-dispersive calibration

of our CCD, 6.5 keV X-rays are digitized to a value of around 250. This value/event could be distributed into more than one pixel, hence the selection of an asymmetric discrimination interval in the next step.

In the left panel of Fig. 1, we show a 250 pixel × 400 pixel region of summed CCD frames after replacing each pixel of each frame with either a 1 or 0 depending on whether its digitized value falls into the interval of 170–270. The right side of the figure shows the result of discriminating against the same range of digitization values, but on cluster values rather than individual pixel values. In addition, *all clusters* of size >3 pixels were also eliminated as probably due to cosmic ray signatures. Fig. 2 compares the spectra derived from these two processed images by column summing the pixel values for the regions shown plus an additional 400 contiguous pixel rows for better statistics. Before column summing, the image was rotated 1° since the CCD columns were not exactly perpendicular to the plane of dispersion established by the orientation of crystal planes. Note that 45° muon tracks remain in the right frame; these could be removed by extending the cluster algorithm to also seek along diagonal directions.

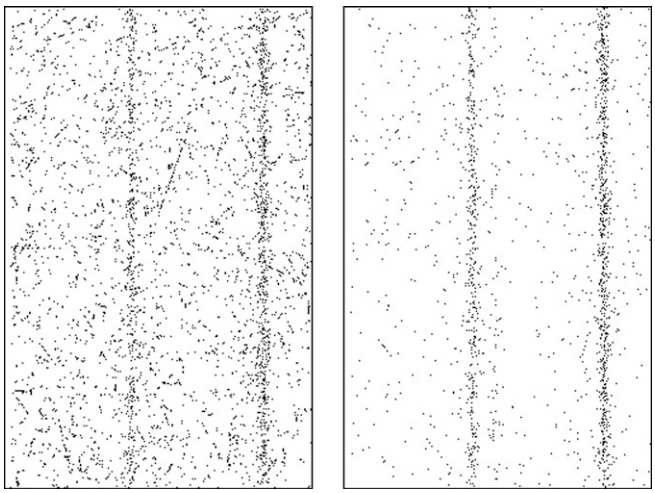

Fig. 1. A 250 pixel × 400 pixel region of the CCD image, before (left) and after (right) applying the cluster algorithm described herein.

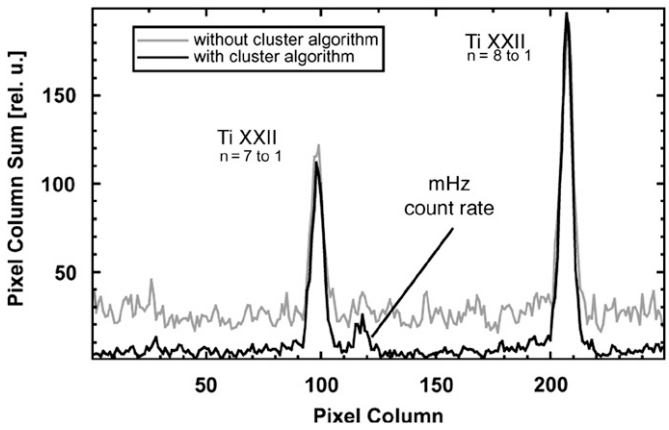

Fig. 2. X-ray spectra due to summing values within each CCD pixel column, before and after accounting for and discriminating against cluster value and size. Note that after application of the spatial–discrimination algorithm, noise is decreased, signal is increased, and the peak labeled "mHz count rate" is now discernible.

4. Discussion

For the present experimental configuration, the source, detector, and crystal geometry were modeled and ray tracing was used to predict the local dispersion. The source-to-crystal distance was 47.2 cm and the crystal-to-detector distance 40.3 cm. The radius of curvature (Rc) of the crystal was determined on the bench using parallel laser beams that focused to Rc/2. For this measurement $\mathrm{Rc} = 223.5\,\mathrm{cm} \pm 1.3\,\mathrm{cm}$. Ray tracing gives a dispersion of 0.29 eV/pixel; this number is robust at the level of two significant figures to within dimensional measurement uncertainties. The two bright peaks in the spectrum were fit to Gaussian functions and are separated by 108.6 pixels, or 31.5 eV calculated using the dispersion and nominal pixel size of 22.5 μm. These peaks are found to be less than 2 eV wide, characteristic of resonant transitions in highly charged ions. Their energy separation compares quite favorably with the 31.6 eV separation of the $n = 8$ to 1 and $n = 7$ to 1 resonance lines of hydrogen-like Ti (using the corresponding spin–orbit–split components) from atomic-structure calculations [6,7]. Using this assignment and the local dispersion thus established, the energy of the faint line is extrapolated to be $6496.5\,\mathrm{keV} \pm 0.4\,\mathrm{eV}$, with the peak centroid dominating this estimate of uncertainty. While it is not the intent of this report to pursue identification of this particular faint line, its energy does correspond to a prominent transition in (Nickel-like) Fe XX, a possible trace contaminant in the ion trap.

5. Conclusion

A variety of techniques are available for observing, calibrating, and identifying features within high-resolution X-ray spectra. We present here a set that finds utility in cases where high resolution, good signal-to-noise, and moderate precision are needed within a low-signal, high-background environment. In particular, the present example required that energy– and wavelength–dispersive spectroscopy be combined with spatial discrimination of clusters to observe and determine the energy of a faint X-ray feature with intensity on the order of the cosmic-ray background in our spectra.

For practical reasons, techniques for very high-precision wavelength determination (not detailed here) are usually reserved for more intense X-ray transitions. Nevertheless, the observation and identification of faint features in X-ray spectra can provide insight into important atomic processes

where asymmetrical branching ratios favor non-radiative decay channels.

References

[1] G.E. Holland, C.N. Boyer, J.F. Seely, J.N. Tan, J.M. Pomeroy, J.D. Gillaspy, Rev. Sci. Instrum. 76 (2005) 073304.
[2] A. Henins, Rev. Sci. Instrum. 58 (1987) 1173.
[3] S. Brennan, P.L. Cowan, R.D. Deslattes, A. Henins, D. Lindle, B.A. Karlin, Rev. Sci. Instrum. 60 (1989) 2243; D. Paterson, C.T. Chantler, C.Q. Tran, L.T. Hudson, F.G. Serpa, R.D. Deslattes, Phys. Scripta T 73 (1997) 400.
[4] D. Groom, Exp. Astronomy 14 (2002) 45.
[5] E. Takacs, B. Radics, C.I. Szabo, S. Biri, L.T. Hudson, J. Imrek, B. Juhasz, T. Suta, A. Valek, J. Palinkas, Nucl. Instr. and Meth. B 235 (2005) 120.
[6] M.F. Gu, in AIP Proceedings 730 (2004) 127.
[7] G.W. Erickson, J. Chem. Ref. Data 6 (1977) 831.